

## Monte Carlo study of the two-dimensional vector Blume-Capel model

Brianna S. Dillon,<sup>1,2</sup> Simone Chiesa,<sup>3,4</sup> and Richard T. Scalettar<sup>3</sup>

<sup>1</sup>*Physics Department, Grove City College, Grove City, Pennsylvania 16127, USA*

<sup>2</sup>*Physics Department, Purdue University, West Lafayette, Indiana 47907, USA*

<sup>3</sup>*Physics Department, University of California, Davis, California 95616, USA*

<sup>4</sup>*Department of Physics and Astronomy, The University of Tennessee, 1408 Circle Drive, Knoxville, Tennessee 37996-1200, USA*

(Received 18 September 2010; published 17 November 2010)

The Blume-Capel model (BCM) generalizes the Ising model to allow for the presence of vacancy sites, and was used as an early description of the effect of a <sup>3</sup>He admixture on the <sup>4</sup>He superfluid transition, especially tricritical behavior. The vector counterpart of the BCM improves upon the original by utilizing spins with a continuous symmetry, the correct universality class for superfluidity. This paper presents a Monte Carlo calculation of the full phase diagram of the two-dimensional vector BCM. A tricritical point is shown to separate a first-order phase transition line at low temperature from a Kosterlitz-Thouless boundary at higher temperature and the location of the tricritical point is determined.

DOI: [10.1103/PhysRevB.82.184421](https://doi.org/10.1103/PhysRevB.82.184421)

PACS number(s): 75.10.Hk, 75.40.Mg, 67.60.G–

### I. INTRODUCTION

It is well known that statistical mechanical systems with three or more components can exhibit the tricritical behavior<sup>1</sup> which characterizes a number of experimental systems, including <sup>3</sup>He-<sup>4</sup>He mixtures<sup>2–4</sup> and metamagnets.<sup>5</sup> In the case of <sup>3</sup>He-<sup>4</sup>He mixtures, two widely applied theoretical descriptions have been via the Blume-Capel model (BCM)<sup>6,7</sup> and Blume-Emery-Griffiths model (BEGM),<sup>8</sup>

$$E = -J \sum_{\langle ij \rangle} S_i S_j - K \sum_{\langle ij \rangle} S_i^2 S_j^2 + D \sum_i S_i^2. \quad (1)$$

Here  $E$  is the energy of a set of classical spins  $S_i$  located at spatial lattice sites  $\mathbf{i}$ . The  $S_i$  have three discrete values,  $S_i = 0, \pm 1$ . This provides a generalization of the Ising model, where  $S_i = \pm 1$ , to allow vacancies,  $S_i = 0$ . The BEGM and BCM allow an understanding of how such spin dilution affects the conventional Ising magnetic transition and provide an analogy to the disruption of the <sup>4</sup>He superfluid transition by an admixture of <sup>3</sup>He. As in the Ising case, the parameter  $J$  describes the coupling between near-neighbor spins on the lattice.  $D$  controls the density of impurities. In addition,  $K$  is a biquadratic term incorporating the difference between <sup>3</sup>He-<sup>3</sup>He and <sup>3</sup>He-<sup>4</sup>He interaction energies. The BCM sets the biquadratic term  $K=0$ .

After their introduction, the BCM and BEGM were carefully studied by a variety of approaches, including renormalization group (RG),<sup>9,10</sup> series expansion,<sup>11</sup> mean field,<sup>8</sup> and Monte Carlo<sup>10,12</sup> treatments. Further generalizations, for example, to include  $S_i^2 S_j^2$  terms were used to understand the thermodynamic behavior of ternary fluids.<sup>13</sup> Not only was quantitative understanding provided for certain experimental systems but the BCM and BEGM also provided general insight into critical phenomena in these complex systems.

The BCM and BEGM have attracted continued theoretical interest. The effect of negative biquadratic interactions in the BEG has been explored in Monte Carlo<sup>14</sup> and mean-field theory,<sup>15</sup> and has been shown to produce rich phase diagrams and new types of phases, e.g., “staggered quadrupolar” regions. Monte Carlo methods such as phenomenological

finite-size scaling,<sup>16</sup> the Monte Carlo renormalization group,<sup>17</sup> and cluster algorithms<sup>18</sup> have allowed increasingly accurate determination of the phase diagrams. Similarly, the topology of the distribution of Lee-Yang zeroes in the case of first-order transitions has been explored,<sup>19</sup> as have been the correlation of fluctuations via  $1/z$  expansions.<sup>20</sup>

In addition to this continuing theoretical work, experiments on systems with tricritical points and their connections to multicomponent statistical mechanical models are also ongoing. These include <sup>3</sup>He-<sup>4</sup>He, metamagnet, and ternary alloy systems. The Blume-Capel model has also been used to understand relaxation dynamics in molecular-based single-chain magnets<sup>21</sup> and hysteresis in FeRh films.<sup>22</sup> New realizations in mixtures of bosonic and fermionic atoms on optical lattices are drawing attention.<sup>23–25</sup>

The original BCM was generalized<sup>26,27</sup> to a vector version,

$$E = -J \sum_{\langle ij \rangle} t_i t_j \cos(\theta_i - \theta_j) + D \sum_i t_i^2, \quad (2)$$

in order better to incorporate the continuous symmetry of the phase of the superfluid wave function. Here the discrete spin  $S_i$  of the BCM Eq. (1) has been replaced by a continuous spin with components  $(\cos \theta_i, \sin \theta_i)$ . A near-neighbor coupling  $-JS_i \cdot S_j$  then gives rise to the first term in Eq. (2).  $\theta_i$  takes on real values  $0 \leq \theta_i < 2\pi$ . The energy scale  $J$  in the vector BCM (VBCM) describes the tendency of the superfluid phase to be uniform at low temperatures while also allowing for vacancies via the variable  $t_i$  which can take the values  $t_i = 0, 1$ . As with  $S_i = 0$  in the initial BCM,  $t_i = 0$  represents sites where no phase variable is present.  $D$  is a vacancy chemical potential. For  $D$  large and negative  $t_i = 1$  on all sites, and the two-dimensional VBCM is equivalent to the planar rotator model. Thus the VBCM generalizes the well-known correspondence between the <sup>4</sup>He superfluid phase transition and the classical planar rotator model, to a <sup>3</sup>He-<sup>4</sup>He mixture.

Initial work<sup>26,27</sup> on the VBCM utilized real-space RG approaches. The RG flows in parameter space introduce an additional coupling  $K \sum_{\langle ij \rangle} t_i t_j$  between vacancies on neighbor-

ing sites, the analog of the term which distinguishes the BCM and BEGM in Eq. (1). The nature of the phase diagram and phase transitions was determined as a function of  $K$ ,  $D$ , and  $T$ .

Recently, the VBCM has been studied for two and three dimensions, and also for both two component spins [the case of Eq. (2)], and three-component spins which are coupled anisotropically.<sup>28–34</sup> A set of studies have put forward strong evidence that, although the introduction of vacancies does cause a region of first-order phase transitions to occur, it does not alter the Kosterlitz-Thouless (KT) critical behavior in other regions of parameter space.<sup>35</sup> In work on the phase diagram of three-dimensional systems, it has been argued that the elucidation of the properties of the VBCM is important to an understanding of experiments on  $^3\text{He}$ - $^4\text{He}$  mixtures confined between two walls.<sup>36–39</sup> The spin dynamics has also been explored and the associated critical exponents at the tricritical point were obtained.<sup>40</sup>

These Monte Carlo studies of the VBCM have focused the nature of the phase transition at *specific* values of  $D$ ,<sup>35</sup> and on the effect of different numbers of components of the order parameter and anisotropies in the coupling. In particular, as noted above, the issue of whether the KT transition survives the presence of vacancies was carefully studied. In this paper, we extend this earlier work by generating the *full* phase diagram of the VBCM in the  $D/J$ - $T/J$  plane (as has also been done very recently for the vector BEGM on a triangular lattice<sup>41</sup>). We show evidence for KT behavior when the vacancy density is low, and first-order transitions at higher dilution, and evaluate the parameters at which first-order character supplants KT behavior. We conclude with a discussion of our results in the context of the RG treatments of the VBCM.

## II. CALCULATIONAL APPROACH

A straightforward implementation of the Metropolis Monte Carlo procedure was employed in which single-spin updates are done of the phase and vacancy variables. More specifically, the entire lattice of phase degrees of freedom was updated followed by a sweep of the vacancies. The autocorrelation time  $\tau$  was monitored via the total magnetization, especially near the phase boundaries, to ensure that measurements were statistically independent. As expected, far from the boundary,  $\tau$  was small, on the order of 2–10 sweeps. Near the phase boundary, on the largest lattice sizes  $\tau \approx 1000$ . For the  $16 \times 16$  lattices we did 10 000 equilibration and 100 000 measurement sweeps. For the  $32 \times 32$  lattices we did 40 000 equilibration and 400 000 measurement sweeps. This factor of 4 increase with a linear lattice size doubling reflects the understanding<sup>42</sup> that the dynamic critical exponent  $z$  of single spin-flip Metropolis simulations of the XY model is approximately  $z=2$ , so that the autocorrelation time scales as  $\tau \propto L^2$ . Our values of  $\tau$  are consistent with those reported in the literature.<sup>42</sup>

Measured observables include the average energy  $\langle E \rangle$  and specific heat  $C = d\langle E \rangle / dT$ , as determined by energy fluctuations, and also the magnetization  $M$  and magnetic susceptibility  $\chi_M$ ,

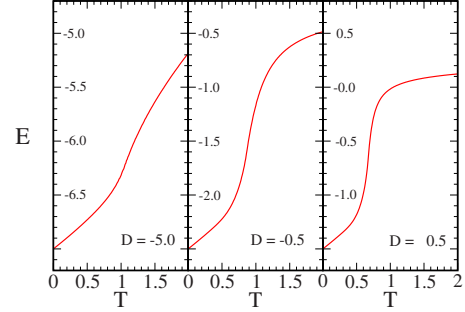


FIG. 1. (Color online) The energy as a function of temperature for different values of the vacancy potential  $D$ . The linear lattice size is  $L=32$ .

$$M = \frac{1}{L^2} \sqrt{M_x^2 + M_y^2},$$

$$M_x = \sum_{\mathbf{i}} \cos \theta_{\mathbf{i}} \quad M_y = \sum_{\mathbf{i}} \sin \theta_{\mathbf{i}},$$

$$\chi_M = L^2 \frac{\langle M^2 \rangle - \langle M \rangle^2}{T}. \quad (3)$$

The vacancy density  $\mathcal{V}$  and vacancy susceptibility  $\chi_{\text{vac}}$ ,

$$\mathcal{V} = \frac{1}{L^2} \sum_{\mathbf{i}} (1 - t_{\mathbf{i}}),$$

$$\chi_{\text{vac}} = L^2 \frac{\langle \mathcal{V}^2 \rangle - \langle \mathcal{V} \rangle^2}{T} \quad (4)$$

provide a signal of the growth in the number of vacancies and their fluctuations, which can occur across a transition into a disordered phase. Here  $L$  is the linear lattice size.

These are also supplemented by a determination of the helicity modulus  $Y_s$ ,

$$\Gamma = \sum_{\mathbf{i}} t_{\mathbf{i}} t_{\mathbf{i}+\hat{x}} \sin(\theta_{\mathbf{i}} - \theta_{\mathbf{i}+\hat{x}}),$$

$$\Lambda = \sum_{\mathbf{i}} t_{\mathbf{i}} t_{\mathbf{i}+\hat{x}} \cos(\theta_{\mathbf{i}} - \theta_{\mathbf{i}+\hat{x}}),$$

$$Y_s = \frac{1}{L^2} \frac{\partial^2 f}{\partial \Delta^2} = \frac{1}{L^2} \left[ \frac{1}{T} (\langle \Gamma^2 \rangle - \langle \Gamma \rangle^2) + \langle \Lambda \rangle \right]. \quad (5)$$

As described in Ref. 43,  $Y_s$  characterizes the response of the free-energy density  $f$  to a phase twist  $\Delta$  applied to the boundaries in the  $\hat{x}$  direction. As is well known,<sup>43</sup> when the temperature-dependent helicity modulus  $Y_s(T)$  intersects the line  $2T/\pi$ , a KT transition between superfluid and nonsuperfluid phases occurs.

Typically, simulations were initiated from random configurations of both spin and vacancy variables. However, as described below, sequences of runs were also performed in which the ending configuration of a simulation at one parameter set was used as the starting configuration of another. The comparison of measurements for cases when a parameter

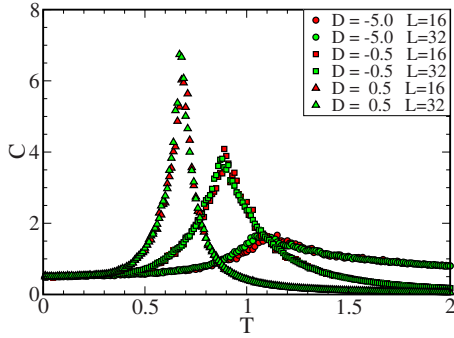


FIG. 2. (Color online) The specific heat  $C$  as a function of temperature for different values of the vacancy potential  $D$  and system size. For a Kosterlitz-Thouless transition, the peak in  $C(T)$  occurs at about 10% higher temperature than  $T_c$ .

was increased with cases when it was decreased allowed for the construction of hysteresis loops which provide a quite accurate determination of the location of first-order transitions, and hence of the tricritical point.

III. RESULTS

A. Energy and specific heat

Figures 1 and 2 show the energy  $E$  and specific heat  $C$  as functions of temperature  $T$  for three different vacancy potentials  $D = -5.0, -0.5, \text{ and } +0.5$ .  $C(T)$  has a maximum which is known for the Kosterlitz-Thouless transition of the planar rotator model to occur at a temperature close to, but roughly 10% above, the critical temperature  $T_c$ . The position of the maxima, like  $T_c$  itself, shifts downward as  $D$  increases and more vacancies are present.  $D = 0.5$  is approaching the tricritical point where the transition becomes first order.

B. Magnetic and vacancy susceptibility

Likewise, Figs. 3 and 4 show the magnetic and vacancy susceptibilities [Eqs. (3) and (4)] as functions of  $T$  for the same values of the impurity potential  $D$  as in Figs. 1 and 2. These measurements also indicate the downward shift in the tendency toward ordering as the vacancy potential  $D$  rises.

Since the phase boundary turns over sharply and runs almost parallel to the  $T$  axis as  $D$  increases further (see Fig. 9),

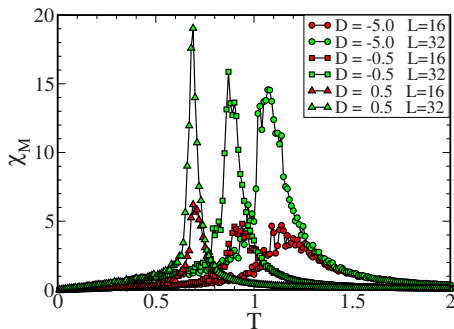


FIG. 3. (Color online) The magnetic susceptibility  $\chi_M$  as a function of temperature for different values of the vacancy potential  $D$  and system size.

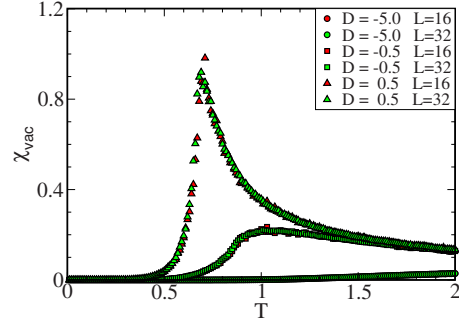


FIG. 4. (Color online) The vacancy susceptibility  $\chi_{vac}$  as a function of temperature for different values of the vacancy potential  $D$  and system size.

it is convenient to examine sweeps of the vacancy concentration  $\mathcal{V}$  as a function of  $D$  at fixed  $T$ .  $\mathcal{V}$  is given for  $T = 0.5, 0.4, \text{ and } 0.01$  in Fig. 5. Data were generated by ramping up  $D$  starting each new simulation at the ending configuration of the preceding one.  $D$  was then decreased back downward. For  $T = 0.5$  (and any larger  $T$  for which the phase boundary is crossed) the increasing and decreasing curves coincide. There is no hysteresis. For  $T = 0.4$  and  $T = 0.01$  the values of  $\mathcal{V}$  depend on whether the starting point was within the ordered or disordered phase. This hysteresis is indicative of a first-order transition. Figure 6 provides a more precise location of the onset of first-order behavior: no hysteresis is present for  $T = 0.42$ , yet clearly occurs for  $T = 0.41$ .

The width  $\Delta D = 4J$  of the hysteresis loop at low  $T$  in Fig. 5 is understood as follows: Beginning with a perfectly ordered phase for which  $t_i = 1$  on all sites and  $\theta_i = \text{constant}$ , the energy cost to insert a vacancy is  $4J$ , since in two dimensions the coordination number is  $z = 4$ . At very low  $T$  this provides a barrier to the introduction of defects. This hysteresis is centered at the transition between the  $T = 0$  energy per site of the perfectly ordered phase,  $E_{\text{ordered}}(T = 0, D)/L^2 = -2J - D$ , and that of the empty lattice,  $E_{\text{empty}}(T = 0, D)/L^2 = 0$ , which occurs at  $D = 2J$ .

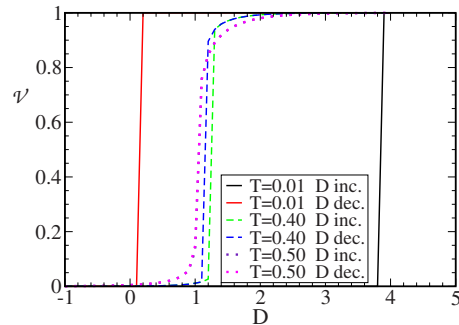


FIG. 5. (Color online) The vacancy density  $\mathcal{V}$  is shown as a function of chemical potential  $D$  at fixed  $T = 0.01, 0.4, \text{ and } 0.5$  (solid, dashed, and dotted curves, respectively). Data are generated by starting in the ordered phase at low  $D$  and gradually increasing  $D$ , initializing each new simulation at the ending configuration of the preceding one. A similar ramp down from the ordered phase is also shown. Hysteresis in  $\mathcal{V}$  is clearly present at  $T = 0.01, 0.4$  (solid and dashed), but not at  $T = 0.5$ , where the two dotted curves coincide. The lattice size  $L = 16$ .

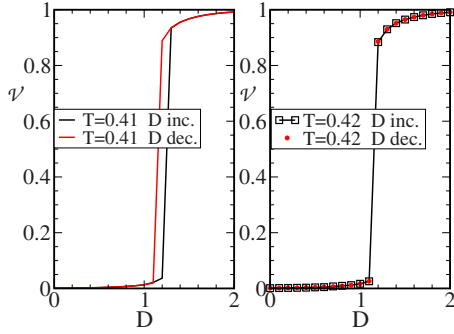


FIG. 6. (Color online) Same as Fig. 5: the vacancy density  $\nu$  is shown as a function of chemical potential  $D$  except here at fixed  $T=0.41$  (left) and  $T=0.42$  (right). Hysteresis is present for  $T=0.41$  but not  $T=0.42$ . The lattice size  $L=16$ .

The first-order regime which is signaled by the opening of the hysteresis loops corresponds to the coexistence (phase separation) of superfluid and normal phases. In the conclusion, we will discuss this point further, as well as the relationship of our findings here and those of the RG treatments.<sup>26,27</sup>

### C. Superfluid stiffness

The superfluid phase transition can also be picked up by the helicity modulus and the crossing condition of  $Y_s(T)$  with the line  $2T/\pi$  discussed in Sec. II. Figures 7 and 8 show  $Y_s(T)$  versus the temperature for different values of  $D$ . Figure 7 fixes  $D=-10.0, -2.0, -1.0, 0.0, 0.4$ , and  $0.9$  for linear lattice size  $L=16$  while Fig. 8 has  $D=-5.0, -0.5$ , and  $0.5$  and  $L=16, 20$ , and  $32$ . At large negative  $D$ , very few vacancies are present, and the crossing  $Y_s(T_c)=2T_c/\pi$  occurs at the highest critical temperature  $T_c$ . As  $D$  increases the critical temperature falls. Eventually, the shape of the  $Y_s(T)$  curve changes qualitatively ( $D=0.9$ ) which corresponds to entry into the region of first-order transitions as seen by the appearance of hysteresis in Figs. 5 and 6. As commented earlier, the critical temperatures inferred from the superfluid density are somewhat below the corresponding peaks in the specific heat and magnetic susceptibility.

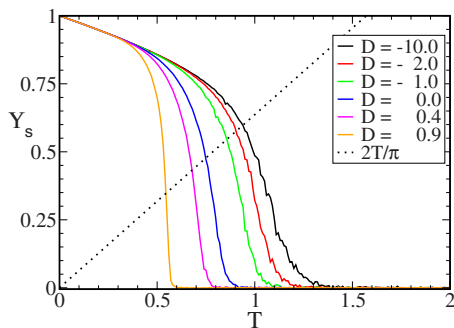


FIG. 7. (Color online) Helicity modulus  $Y_s$  versus  $T$  for different  $D=-10, -2, -1, 0, 0.4$ , and  $0.9$ . At low  $D$ , the crossing of the line  $2T/\pi$  gives the position of the KT transition (see text). Eventually, for  $D$  large, the transition becomes first order, as is best seen by the development of hysteresis in the vacancy density (Figs. 5 and 6).

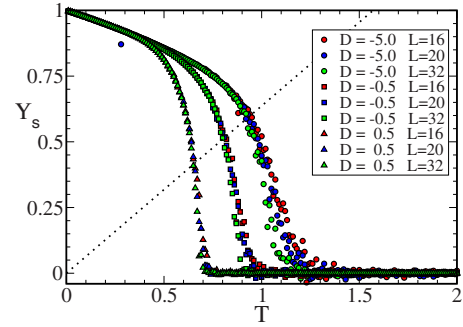


FIG. 8. (Color online) Same as Fig. 7 except  $D=-5, -0.5$ , and  $0.5$ . Data for different lattice sizes  $L=16, 20$ , and  $32$  are compared.

Figure 8 provides an indication of finite-size effects. The crossing point moves somewhat downward in temperature as linear lattice size increases from  $L=16$  to  $L=32$ . For  $D$  large and negative, the planar rotator model, we find the crossing at  $T \approx 0.94$  for  $L=16$  and  $T \approx 0.92$  for  $L=32$ . In the thermodynamic limit, the planar rotator transition temperature is known to quite high accuracy,  $T_c=0.892$ .<sup>44</sup> Note that the finite-size effects are quite small in the specific heat and vacancy susceptibility, Figs. 2 and 4, but more significant in the magnetic susceptibility, Fig. 3.

### D. Phase diagram

The results for the superfluid stiffness and the hysteresis in the vacancy density can be put together to determine the phase diagram of the VBCM. This is shown in Fig. 9. For  $D$  large and negative, the data indicate a Kosterlitz-Thouless transition from a superfluid to normal phase at  $T_c \approx 0.90$ , when data for  $L=16-32$  are extrapolated to the thermodynamic limit. This agrees to within 1% with existing values,  $T_c=0.892$ .<sup>44</sup>

This nearly vertical phase boundary begins to turn over as  $D$  approaches  $D=-2$ , and then begins to run almost horizontally, so that  $T_c$  quickly goes to zero. At the tricritical point  $T=0.40 \pm 0.02$ ,  $D=1.15 \pm 0.05$ , the nature of the transition

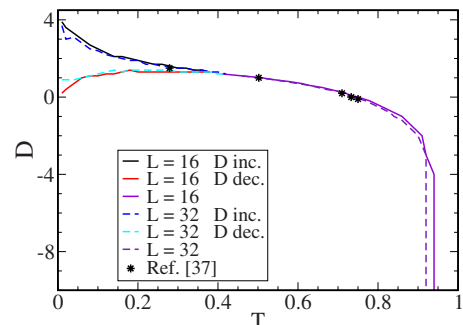


FIG. 9. (Color online) Phase diagram showing the boundary between the ordered phase of the vector Blume-Capel model at low  $T$  and  $D$  and the high  $T$  and  $D$  disordered phase. There is a tricritical point at  $T=0.40 \pm 0.02$ ,  $D=1.15 \pm 0.05$  which separates first-order transitions at low  $T$  from Kosterlitz-Thouless ones at higher  $T$ . Data are provided for  $L=16$  and  $L=32$ , and also compared with the critical points obtained by Romano *et al.* (Ref. 35).

changes from KT to first order. A coexistence of superfluid and normal fluid exists in the regions shown. Results are in good agreement with previous data of Chamati *et al.*<sup>35</sup>

#### IV. CONCLUSION

The Blume-Capel and Blume-Emery-Griffiths models extended the consideration of critical phenomena for saturated lattices to the case of lattice gases which include both magnetic and vacancy degrees of freedom. In its vector version, the VBCM provides a description of the effect of <sup>3</sup>He vacancies on the <sup>4</sup>He superfluid transition which incorporates the correct continuous symmetry of the order parameter.

This paper has extended previous Monte Carlo studies of the VBCM at specific values of parameter space to generate the phase diagram in the entire  $D$ - $T$  plane. The position of the tricritical point which separates the KT phase transitions at small vacancy density from a first-order boundary at higher vacancy fractions was found to be  $(D/J)_{\text{tcp}} = 1.15 \pm 0.05$ ,  $(T/J)_{\text{tcp}} = 0.40 \pm 0.02$ . This location was obtained by examining hysteresis in the vacancy density as the chemical potential is changed. Such a determination is somewhat sensitive to the lattice size, nature of the Monte Carlo moves, and length of the runs. Simulations with different choices for these parameters resulted in the error bars indicated.

Early real-space RG studies of the VBCM suggested that there was no tricritical point in two dimensions.<sup>26,27</sup> Instead, as the critical temperature drops due to greater vacancy concentration, the KT transition is first replaced by phase separation

into two normal phases. Only at yet lower temperatures does a region of superfluid-normal coexistence occur. These studies, however, considered models which include an analog,  $K\sum_{\langle ij \rangle} t_i t_j$ , of the biquadratic term in the BEGM. This term appears in the RG flows of the VBCM even if not present in the original expression for the VBCM energy. Reference 27 discusses the effect of  $K$  on the size of the region of phase separation between two normal fluids. The authors emphasize that, when  $K=0$  and the VBCM is recovered, the region is very small, extending over values of  $T$  of only 1–2 %. The very small size of this region leads them to refer to the presence of an “effective tricritical point”  $T_e$ , consistent with our findings here.

Indeed, although the phases of the full BEGM and VBCM for general  $K$  are very interesting, in many cases the value of  $K$  is believed to be relatively small, as first discussed in Ref. 8. In this case, we suggest here in agreement with Ref. 27, that there is a tricritical point of the VBCM, as is known to exist in the discrete models with three components. As a final comment, it is worth noting that in three dimensions Monte Carlo simulations of the VBCM provide unambiguous evidence for a tricritical point.<sup>45,46</sup>

#### ACKNOWLEDGMENTS

The work of Brianna Dillon was funded by the National Science Foundation Research Experience for Undergraduate program under Grant No. PHY-0649297. The project was also supported under ARO under Award No. W911NF0710576 with funds from the DARPA OLE Program.

- 
- <sup>1</sup>R. B. Griffiths and B. Widom, *Phys. Rev. A* **8**, 2173 (1973).  
<sup>2</sup>E. H. Graf, D. M. Lee, and J. D. Reppy, *Phys. Rev. Lett.* **19**, 417 (1967).  
<sup>3</sup>G. Goellner and H. Meyer, *Phys. Rev. Lett.* **26**, 1534 (1971).  
<sup>4</sup>G. Ahlers, in *The Physics of Liquid and Solid Helium*, edited by J. B. Ketterson and K. H. Bennemann (Wiley, New York, 1974).  
<sup>5</sup>V. A. Schmidt and S. A. Friedberg, *Phys. Rev. B* **1**, 2250 (1970).  
<sup>6</sup>M. Blume, *Phys. Rev.* **141**, 517 (1966).  
<sup>7</sup>H. W. Capel, *Physica (Utrecht)* **32**, 966 (1966).  
<sup>8</sup>M. Blume, V. J. Emery, and R. B. Griffiths, *Phys. Rev. A* **4**, 1071 (1971).  
<sup>9</sup>A. N. Berker and M. Wortis, *Phys. Rev. B* **14**, 4946 (1976).  
<sup>10</sup>T. W. Burkhardt and H. J. F. Knops, *Phys. Rev. B* **15**, 1602 (1977).  
<sup>11</sup>D. M. Saul, M. Wortis, and D. Stauffer, *Phys. Rev. B* **9**, 4964 (1974).  
<sup>12</sup>A. K. Jain and D. P. Landau, *Phys. Rev. B* **22**, 445 (1980).  
<sup>13</sup>D. Mukamel and M. Blume, *Phys. Rev. A* **10**, 610 (1974).  
<sup>14</sup>Y.-L. Wang, F. Lee, and J. D. Kimel, *Phys. Rev. B* **36**, 8945(R) (1987).  
<sup>15</sup>W. Hoston and A. N. Berker, *Phys. Rev. Lett.* **67**, 1027 (1991).  
<sup>16</sup>P. D. Beale, *Phys. Rev. B* **33**, 1717 (1986).  
<sup>17</sup>D. P. Landau and R. H. Swendsen (unpublished).  
<sup>18</sup>A. Rachadi and A. Benyoussef, *Phys. Rev. B* **68**, 064113 (2003).  
<sup>19</sup>M. Biskup, C. Borgs, J. T. Chayes, L. J. Kleinwaks, and R. Kotecky, *Phys. Rev. Lett.* **84**, 4794 (2000).  
<sup>20</sup>K. G. Moter and R. S. Fishman, *Phys. Rev. B* **45**, 5307 (1992).  
<sup>21</sup>J. I. Kishine, T. Watanabe, H. Deguchi, M. Mito, T. Sakai, T. Tajiri, M. Yamashita, and H. Miyasaka, *Phys. Rev. B* **74**, 224419 (2006).  
<sup>22</sup>S. Maat, J.-U. Thiele, and E. E. Fullerton, *Phys. Rev. B* **72**, 214432 (2005).  
<sup>23</sup>H. Ott, E. de Mirandes, F. Ferlaino, G. Roati, G. Modugno, and M. Inguscio, *Phys. Rev. Lett.* **92**, 160601 (2004).  
<sup>24</sup>K. Günter, T. Stöferle, H. Moritz, M. Köhl, and T. Esslinger, *Phys. Rev. Lett.* **96**, 180402 (2006).  
<sup>25</sup>S. Ospelkaus, C. Ospelkaus, L. Humbert, K. Sengstock, and K. Bongs, *Phys. Rev. Lett.* **97**, 120403 (2006).  
<sup>26</sup>J. L. Cardy and D. J. Scalapino, *Phys. Rev. B* **19**, 1428 (1979).  
<sup>27</sup>A. N. Berker and D. R. Nelson, *Phys. Rev. B* **19**, 2488 (1979).  
<sup>28</sup>S. Romano and R. O. Sokolovskii, *Phys. Rev. B* **61**, 11379 (2000).  
<sup>29</sup>H. Chamati and S. Romano, *Phys. Rev. B* **72**, 064424 (2005).  
<sup>30</sup>H. Chamati and S. Romano, *Phys. Rev. B* **72**, 064444 (2005).  
<sup>31</sup>H. Chamati and S. Romano, *Phys. Rev. B* **73**, 184424 (2006).  
<sup>32</sup>A. C. D. van Enter, S. Romano, and V. A. Zagrebnov, *J. Phys. A* **39**, L439 (2006).  
<sup>33</sup>H. Chamati and S. Romano, *Eur. Phys. J. B* **54**, 249 (2006).  
<sup>34</sup>L. A. S. Mól, A. R. Pereira, H. Chamati, and S. Romano, *Eur. Phys. J. B* **50**, 541 (2006).

- <sup>35</sup>H. Chamati and S. Romano, *Phys. Rev. B* **75**, 184413 (2007).
- <sup>36</sup>R. Garcia and M. H. W. Chan, *Phys. Rev. Lett.* **83**, 1187 (1999).
- <sup>37</sup>R. Garcia and M. H. W. Chan, *Phys. Rev. Lett.* **88**, 086101 (2002).
- <sup>38</sup>T. Ueno, S. Balibar, T. Mizusaki, F. Caupin, and E. Rolley, *Phys. Rev. Lett.* **90**, 116102 (2003).
- <sup>39</sup>T. Ueno, S. Balibar, T. Mizusaki, F. Caupin, M. Fechner, and E. Rolley, *J. Low Temp. Phys.* **130**, 543 (2003).
- <sup>40</sup>J. A. Plascak, S.-H. Tsai, and D. P. Landau, *Phys. Rev. E* **76**, 011105 (2007).
- <sup>41</sup>J. B. Santos-Filho, J. A. Plascak, and D. P. Landau, *Physica A* **389**, 2934 (2010).
- <sup>42</sup>J. F. Fernández, M. F. Ferreira, and J. Stankiewicz, *Phys. Rev. B* **34**, 292 (1986).
- <sup>43</sup>G. M. Wysin, A. R. Pereira, I. A. Marques, S. A. Leonel, and P. Z. Coura, *Phys. Rev. B* **72**, 094418 (2005).
- <sup>44</sup>P. Olsson, *Phys. Rev. B* **52**, 4526 (1995).
- <sup>45</sup>A. Maciołek, M. Krech, and S. Dietrich, *Phys. Rev. E* **69**, 036117 (2004).
- <sup>46</sup>R. T. S. Freire, S. J. Mitchell, J. A. Plascak, and D. P. Landau, *Phys. Rev. E* **72**, 056117 (2005).